

Structural basis for arabinxylo-oligosaccharide capture by the probiotic *Bifidobacterium animalis* subsp. *lactis* Bl-04

Morten Ejby,¹ Folmer Fredslund,^{1,2}

Andreja Vujicic-Zagar,³ Birte Svensson,¹

Dirk Jan Slotboom³ and Maher Abou Hachem^{1*}

¹Enzyme and Protein Chemistry, Department of Systems Biology, Technical University of Denmark, Søltofts Plads, Building 224, DK-2800 Kgs. Lyngby, Denmark.

²MAX-lab, MAX IV Laboratory, Lund University, Ole Römers väg 1, 223 63 Lund, Sweden.

³Membrane Enzymology, Institute for Biomolecular Sciences & Biotechnology, Rijksuniversiteit Groningen, Nijenborgh 4, 9747 AG Groningen, The Netherlands.

Summary

Glycan utilization plays a key role in modulating the composition of the gut microbiota, but molecular insight into oligosaccharide uptake by this microbial community is lacking. Arabinxylo-oligosaccharides (AXOS) are abundant in the diet, and are selectively fermented by probiotic bifidobacteria in the colon. Here we show how selectivity for AXOS uptake is established by the probiotic strain *Bifidobacterium animalis* subsp. *lactis* Bl-04. The binding protein *BlAXBP*, which is associated with an ATP-binding cassette (ABC) transporter that mediates the uptake of AXOS, displays an exceptionally broad specificity for arabinosyl-decorated and undecorated xylo-oligosaccharides, with preference for tri- and tetra-saccharides. Crystal structures of *BlAXBP* in complex with four different ligands revealed the basis for this versatility. Uniquely, the protein was able to recognize oligosaccharides in two opposite orientations, which facilitates the optimization of interactions with the various ligands. Broad substrate specificity was further enhanced by a spacious binding pocket accommodating decorations at different mainchain positions and conformational flexibility of a lid-like loop. Phylogenetic and genetic analyses show that *BlAXBP* is highly conserved within *Bifidobacterium*, but is lacking in other gut microbiota members. These

data indicate niche adaptation within *Bifidobacterium* and highlight the metabolic syntrophy (cross-feeding) among the gut microbiota.

Introduction

The human gastrointestinal tract (GIT) hosts a highly diverse microbial community referred to as the gut microbiota (Eckburg *et al.*, 2005) that comprises one of the most densely populated ecological niches in nature (Xu *et al.*, 2007). Despite the dynamic nature and diversity of the gut microbiota, only four bacterial phyla dominate this community, with Firmicutes being the most abundant followed by Bacteroidetes, Actinobacteria and Proteobacteria (Arumugam *et al.*, 2011). The *Bifidobacterium* genus is prevalent among gut Actinobacteria. *Bifidobacterium* is physiologically important as it harbours several probiotic (health promoting) strains able to improve bowel function, prevent or alleviate infectious diarrhoea, certain metabolic disorders and inflammatory conditions (e.g. Crohn's disease) as well as confer host resistance against colonization of pathogens (Picard *et al.*, 2005; Wallace *et al.*, 2011). An important characteristic of probiotic bacteria is their ability to utilize a variety of oligosaccharides that are indigestible by the human host (Koropatkin *et al.*, 2012).

Arabinoxylan, comprising a β -(1,4)-linked xylosyl backbone decorated with arabinosyl sidechains (Biely, 2012), is the second most abundant non-starch polysaccharide in cereal grains, mounting to 25–40% (w/w) of the dietary fibre content (Nyman *et al.*, 1984). The only currently known gut xylanolytic taxa are *Bacteroides* and *Roseburia* strains that produce extracellular endo-xylanases able to hydrolyse the backbone of this polysaccharide. The action of these endo-xylanases, which are classified into glycoside hydrolase family 10 (GH10) according to the sequence and mechanism-based CAZy classification (<http://www.cazy.org>) produces both undecorated xylo-oligosaccharides (XOS) and arabinosyl decorated arabinxylo-oligosaccharides (AXOS) (see Fig. 1 for examples), which become accessible to cross-feeding species of secondary glycan degraders (Flint *et al.*, 2007). Growth on XOS is limited to a few taxa among the gut microbiota, e.g. bifidobacteria and some *Lactobacillus brevis* strains (Crittenden *et al.*, 2002), but several commensals and potential pathogens, e.g. members of the

Accepted 30 September, 2013. *For correspondence. E-mail maha@bio.dtu.dk; Tel. (+45) 45252732, (+45) 45252731; Fax (+45) 45886307.

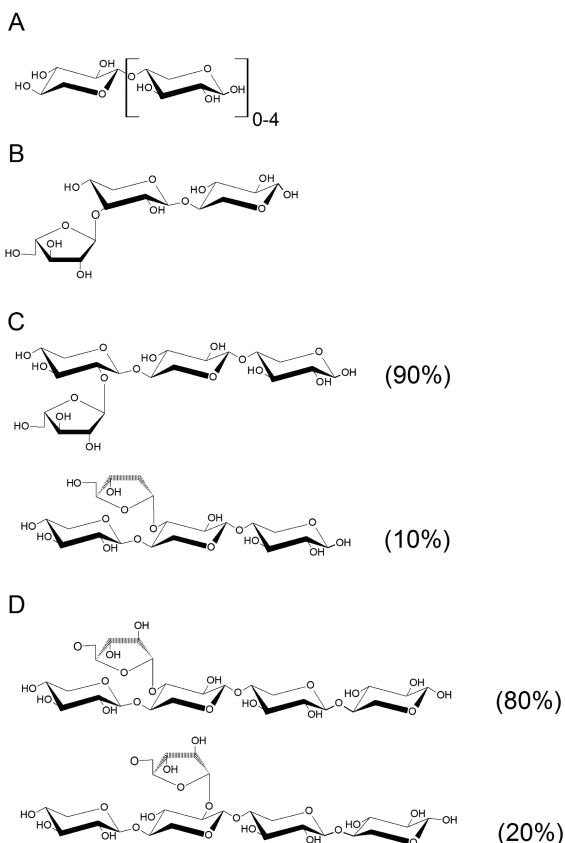


Fig. 1. Structures of the xylo-oligosaccharide and arabinoxyl-oligosaccharide ligands used in this study. The arabinoxyl-oligosaccharide ligands arabinoxylotriose and arabinoxylotetraose are mixtures and the percentages indicated denote the (w/w) proportions as described in *Experimental procedures*. (A) Xylobiose through to xylohexaose, (B) arabinoxylbiose, (C) arabinoxylotriose, (D) arabinoxylotetraose.

Clostridium and *Escherichia* genera are unable to utilize these oligosaccharides (Moura *et al.*, 2007).

Bifidobacteria have been shown to grow more efficiently on XOS and AXOS than on the monosaccharide xylose (Palframan *et al.*, 2003), indicative of a specific transport system for these glycans. Notably, the counts of *Bifidobacterium animalis* subsp. *lactis* were specifically increased in a colon simulator study (Mäkeläinen *et al.*, 2010) when XOS was supplemented instead of the well-established prebiotic fructo-oligosaccharides (FOS). A similar increase in bifidobacterial counts was observed *in vivo* in mice (Hansen *et al.*, 2013), emphasizing selective fermentation of XOS by members of this genus.

The AXOS utilization locus in *B. animalis* subsp. *lactis* BI-04 encodes a LacI transcriptional regulator, glycoside hydrolases and esterases involved in the degradation of AXOS, as well as an ATP-binding cassette (ABC) transporter (Andersen *et al.*, 2013). The ABC transport system of this locus is conserved across different XOS-utilizing

species within *Bifidobacterium*, but currently the molecular features of AXOS uptake are unknown. ABC importers consist of two transmembrane domains (TMDs) forming the translocation pore, two intracellular nucleotide binding domains that power the transport process by harnessing energy from ATP hydrolysis, and an extracellular (or periplasmic) solute binding protein (SBP) that governs the specificity and high-affinity capture of substrates (Davidson *et al.*, 2008). This modular organization is also valid for the AXOS utilization locus in *B. animalis* subsp. *lactis* BI-04, although the gene encoding the ATP-binding protein (locus tag number: Balac_1610) is not a part of the locus as it was suggested to energize several glycan-specific ABC systems in this organism based on whole-genome microarray transcriptional analysis (Andersen *et al.*, 2013).

Here, we describe the kinetics and energetics of the binding of arabinoxylan derived oligosaccharides to the SBP encoded in the AXOS locus in *B. animalis* subsp. *lactis* BI-04. In addition, crystal structures of this binding protein in complex with undecorated (XOS) and arabinosyl decorated (AXOS) ligands are determined disclosing the molecular features of AXOS capture. These data bring novel insight into the molecular basis of AXOS uptake by probiotic bifidobacteria and advance the understanding of xylan metabolism and syntrophy (cross feeding) between different groups of the gut microbiota.

Results

Production and purification of recombinant xylo-oligosaccharide binding protein from *B. animalis* subsp. *lactis* (BIAXBP)

Recently, the ABC transport system that confers the uptake of xylo-oligosaccharides was tentatively identified by whole-genome microarrays transcriptional analysis (Andersen *et al.*, 2013). The balac_0514 gene fragment encoding the mature solute-binding protein of this ABC transport system, designated as BIAXBP, was cloned into an expression vector for production in *Escherichia coli*. Recombinant BIAXBP was purified at yields of ~ 2.5 mg·g⁻¹ cell wet weight.

Specificity and affinity of BIAXBP

Binding of BIAXBP to XOS with a degree of polymerization (DP) 2–6, and AXOS of DP 3–5 (Fig. 1) as well as to eight other mono-, di- and oligosaccharides was analysed by surface plasmon resonance. Only XOS and AXOS resulted in significant response at the tested concentrations, which enabled discerning the kinetics of ligand binding (Fig. 2). BIAXBP displayed highest affinity towards xylotetraose with a $K_d = 45$ nM, followed closely by arabinoxylotriose,

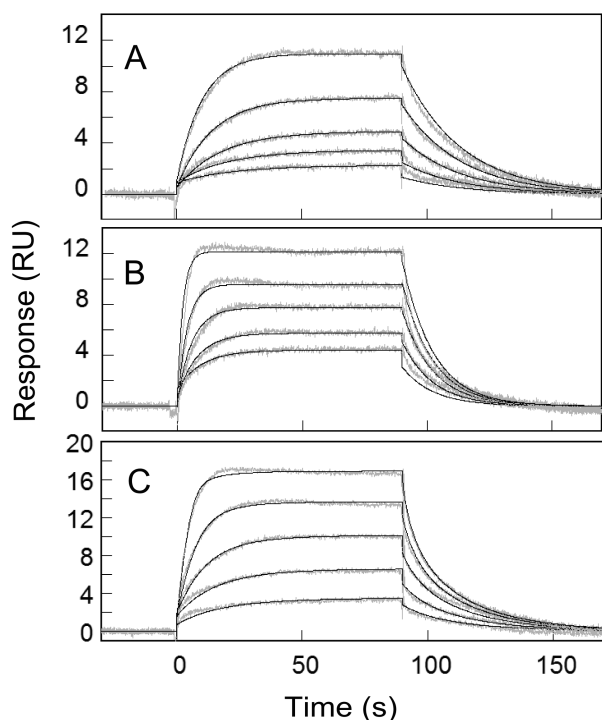


Fig. 2. Binding kinetics of XOS to BAXBP as analysed by surface plasmon resonance at 25°C in 20 mM phosphate/citrate, 150 mM NaCl pH 6.5, 0.005% (v/v) P20 surfactant. Blank and reference cell corrected sensograms (grey) and one binding site global fits (solid black lines) to five ligand concentrations: (A) xylotetraose 3.4–57 nM, (B) arabinoxytolriose 19.5–312 nM, (C) xylopentaose 109–1750 nM.

arabinoxylobiose and xylotriose (Table 1, Fig. S1). The affinity dropped steeply for ligands smaller than a trisaccharide or larger than a pentasaccharide owing mainly to a slower association rate constant (k_{on}) except for xylobiose where a faster dissociation rate constant (k_{off}) also contributed to the lower affinity (Table 1, Fig. S1). Arabinosyl decorations were preferred at the non-reducing xyloxy moiety (e.g. arabinoxylobiose and arabinoxytolriose), as judged by the higher affinity as compared to the corresponding unsubstituted ligands. By contrast,

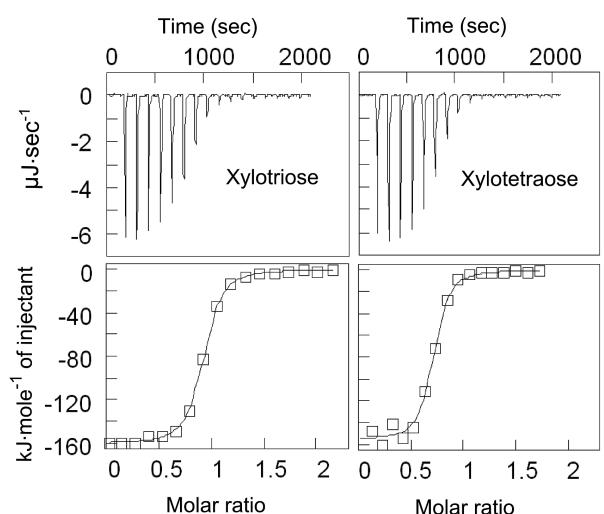


Fig. 3. Isothermal titration calorimetry analysis of BAXBP binding to xylotriose and xylotetraose. The top panel shows the thermograms and bottom graphs depict the binding isotherms and one site binding model fits to the data (solid lines). The analysis is performed at 25°C and pH 6.5 using 250 μM of each ligand in the syringe and 25 μM BAXBP in the cell.

decorations (e.g. arabinoxytoltetraose) resulted in reduced affinity compared to the undecorated ligand (Fig. 1, Table 1, Fig. S1).

The maximum binding affinity of BAXBP for xylotetraose was at pH 6.5–7, but changed only modestly at pH 5–8 (Fig. S2A) consistent with pH in the gut ranging between 5.5 and 7.5 (Kleerebezem and Vaughan, 2009). The affinity of BAXBP to xylotetraose decreased with increasing temperature in the interval 15–30°C mainly due to higher k_{off} (Fig. S2B).

The thermodynamic parameters and binding stoichiometry for xylotriose and xylotetraose were determined using isothermal titration calorimetry (Fig. 3) and revealed a binding process driven by a favourable enthalpy change $\Delta H^\circ = -165 \text{ kJ} \cdot \text{mol}^{-1}$ which was compensated by a large unfavourable binding entropy $T\Delta S^\circ = -126 \text{ kJ} \cdot \text{mol}^{-1}$ (Table 2). The affinity trend and the magnitude of the

Table 1. Kinetics of xylo-oligosaccharide binding to BAXBP as measured by surface plasmon resonance.

Ligand ^a	k_{on} $M^{-1} s^{-1}$	k_{off} s^{-1}	K_d M	χ^2
Xylobiose	$(5.7 \pm 0.20) \times 10^4$	$(5.5 \pm 0.08) \times 10^{-1}$	9.00×10^{-6}	0.11
Xylotriose	$(1.3 \pm 0.02) \times 10^6$	$(1.3 \pm 0.01) \times 10^{-1}$	1.02×10^{-7}	0.10
Xylotetraose	$(1.0 \pm 0.001) \times 10^6$	$(4.6 \pm 0.04) \times 10^{-2}$	4.53×10^{-8}	0.09
Xylopentaose	$(9.0 \pm 0.08) \times 10^4$	$(6.2 \pm 0.03) \times 10^{-2}$	6.57×10^{-7}	0.17
Xylohexaose	$(1.8 \pm 0.01) \times 10^3$	$(4.4 \pm 0.02) \times 10^{-2}$	2.50×10^{-5}	0.19
Arabinoxylobiose	$(6.5 \pm 0.13) \times 10^5$	$(5.2 \pm 0.10) \times 10^{-2}$	8.10×10^{-8}	0.17
Arabinoxytolriose	$(1.1 \pm 0.01) \times 10^6$	$(7.8 \pm 0.04) \times 10^{-2}$	7.08×10^{-8}	0.14
Arabinoxytoltetraose	$(9.0 \pm 0.20) \times 10^4$	$(1.4 \pm 0.03) \times 10^{-1}$	1.55×10^{-6}	0.13

^a Chemical purity, composition and structure are described in *Experimental procedures*.

Table 2. Thermodynamic parameters and binding constants obtained by ITC.

Ligand	ΔG° kJ mol ⁻¹	ΔH° kJ mol ⁻¹	$T\Delta S^\circ$ kJ mol ⁻¹	K_d M	n^d
Xylotriose ^a	-39.1	-165.5	-126.4	1.4×10^{-7}	0.95
Xylotetraose ^a	-39.5	-163.2	-123.7	1.3×10^{-7}	0.83
Xylotriose ^b	-39.9	ND	ND	1.0×10^{-7}	0.75
Xylotetraose ^b	-42.0	ND	ND	4.5×10^{-8}	0.70
Xylotriose ^c	-41.4	ND	ND	7.5×10^{-8}	1.13
Xylotetraose ^c	-40.7	ND	ND	5.7×10^{-8}	1.09

^a Determined by ITC.^b Determined by SPR.^c Determined by fluorescence emission spectroscopy.^d Binding stoichiometry as measured by the different techniques. Binding data from SPR and fluorescence spectroscopy measurements are shown for comparison.

binding constants were in good agreement with SPR and fluorescence spectroscopy measurements (Tables 1 and 2, Fig. S3).

Overall three-dimensional structure

Crystal structures of *BIA*BP in complex with several ligands were solved using the single-anomalous diffraction

(SAD) method to a maximum resolution of 2.0 Å (Table 3). *BIA*BP is classified into cluster B according to the structural alignment classification system and it shares the same overall fold as other solute binding proteins (Berntsson *et al.*, 2010). Accordingly, *BIA*BP comprises two domains of different size joined by a hinge region with the ligand binding site buried at the interface between the two domains (Fig. 4). The N-terminal domain (domain I) (1–143; 318–362) contains seven α -helices and five β -strands, two of which form a part of the hinge region and continue into the larger C-terminal domain (domain II) (147–314; 365–425). Domain II, which is stabilized by a disulphide bridge between Cys209 and Cys227, consists of 11 α -helices and four β -strands. The hinge region comprises two short β -strands arranged in an anti-parallel β -sheet spanning the two domains (144–146; 315–317) and the short loop 363–365 (Fig. 4).

A DALI structure comparison search (Holm and Rosenström, 2010) against the Protein Data Bank (PDB), showed the closest structural homologue to be the recently published solute binding protein from the thermophile *Caldanaerobius polysaccharolyticus* (*Cp*XB1) which is specific to short xylo-oligosaccharides (Han *et al.*, 2012) (PDB code 4g68; Z-score = 46.9; RMSD = 2.0 Å for 379 aligned C_α atoms and 23% sequence identity). Other high

Table 3. Data collection and refinement statistics of the complex structures of *BIA*BP.

	Xylotetraose	Xylotriose	Arabinxylobiose	Arabinxylotriose
Beamline	SLS X06SA	SLS X06SA	MAX-lab I911-3	MAX-lab I911-3
PDB ID	3zkk	3zkl	4c1u	4c1t
Wavelength (Å)	0.979	0.979	1.000	1.000
Resolution range (Å)	45.8–2.2 (2.3–2.2)	45.8–2.4 (2.5–2.4)	28.2–2.0 (2.07–2.0)	32.2–2.39 (2.48–2.39)
Space group	<i>P</i> 2 ₁ 2 ₁ 2			
Unit cell	68.0 124.0 61.3	68.0 124.0 61.3	67.5 96.7 56.3	67.4 96.1 56.7
Unique reflections ^a	27 024 (2590)	20 785 (1861)	25 178 (2484)	14 857 (1318)
Multiplicity ^a	6.6 (6.1)	7.3 (7.5)	4.1 (3.9)	3.9 (3.4)
Completeness (%) ^a	99.5 (97.5)	98.8 (90.1)	98.6 (99.7)	98.27 (89.0)
<i>R</i> -meas (%) ^a	5.6 (152.0)	5.9 (150.9)	7.7 (50.1)	9.3 (66.8)
Mean <i>I</i> / $\sigma(I)$ ^a	17.7 (2.12)	20.9 (2.24)	15.6 (3.46)	13.4 (2.0)
Wilson B-factor	55.6	62.3	23.7	33.6
<i>R</i> -factor ^b	0.20 (0.43)	0.19 (0.37)	0.15 (0.20)	0.21 (0.25)
<i>R</i> -free ^b	0.24 (0.44)	0.24 (0.44)	0.21 (0.25)	0.25 (0.34)
Number of atoms	3173	3164	6225	3100
Macromolecules	3002	3002	3007	3002
Ligands	59	60	92	37
Water	112	102	219	61
Protein residues	396	396	396	396
RMS bonds (Å)	0.008	0.008	0.005	0.005
RMS angles (°)	1.30	1.28	0.76	1.06
Ramachandran favoured (%)	98	98	99	98
Ramachandran outliers (%)	0	0	0	0.25
Clash score	4.32	3.98	1.5	2.0
Average B-factor	32.1	30.3	27.5	43.6
Macromolecules	32.3	30.5	27.0	43.7
Ligands	25.3	31.0	34.3	36.1
Water	28.5	25.3	32.0	41.9

^a Values in the parenthesis are for the highest resolution shell.^b Values in the parenthesis are before refinement.

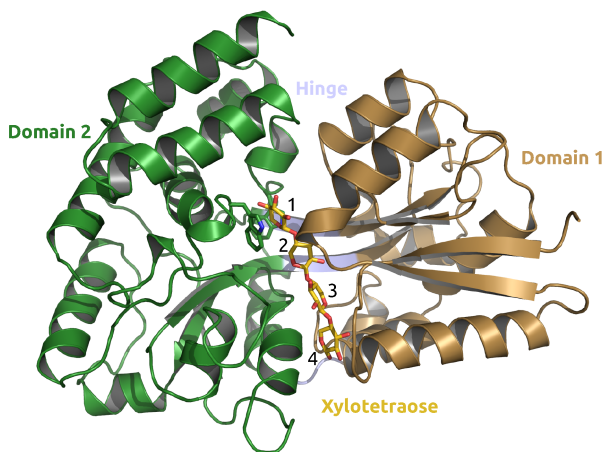


Fig. 4. Ribbon representation of the overall structure of BIAXBP complexed with xylohexose. The protein consists of an N-terminal domain in brown (domain I, residues 30–143 and 318–362) and a larger C-terminal domain in green (domain II, residues 147–314 and 365–425). The two domains are linked by a hinge in light blue (residues 144–146, 315–317 and 363–364).

score hits were carbohydrate-specific SBPs sharing low sequence identities (< 20%) and displaying diverse ligand specificities and taxonomic origin as compared to BIAXBP. The only characterized bifidobacterial SBP (lacto-N-biose SBP from *Bifidobacterium longum*, PDB code 2z8d) had a Z-score of 31.9 and sequence identity of 17% attesting the functional divergence of these taxonomically related SBPs.

Ligand binding site

The crystal structures of BIAXBP in complex with arabinohydroxylobiose, arabinohydroxylotriose, xylotriose and xylohexose show well-defined densities for bound oligosaccharides in the binding site. The preferred ligand xylohexose adopts a helical conformation close to the energetically favoured threefold symmetrical conformation observed in xylan (Nieduszynski and Marchessault, 1971) (Fig. 5A). The mainchain xylosyl units of the ligands are numbered starting with 1 for the terminal xylosyl moiety sandwiched between Trp195 and Trp384 of domain II (Fig. 5, see details below). The arabinosyl substitutions at positions 1 and 2 are denoted with 1' or 2' respectively (Fig. 5C and D). Unsubstituted XOS ligands were modelled with the non-reducing end at position 1 (Fig. 5A and B), although binding of these ligands in the opposite directionality (i.e. with the reducing end xylosyl at position 1) is equally feasible as the only difference between the oppositely oriented molecules is the position of the xylosyl ring oxygen (Fig. S4).

All the mainchain xylosyl moieties of xylotriose and xylohexose are recognized by the protein. Xylosyl units 1

and 2 are bound by both polar interactions and aromatic stacking, whereas polar interactions shape the binding to the units at positions 3 and 4. The sugar units at positions 1 and 4 make most direct interactions, consistent with maximal affinity for xylohexose, and tolerance for side-chain decorations at positions 1 and 2 (Fig. 5). In more detail: xylose unit 1 stacks onto Trp195 and Trp384 and additionally makes polar interactions with Asn72, His199 and Asp386 (Fig. 5A and B). Xylose unit 2 stacks onto Trp277 and makes polar contacts to Asn39, and Gln254, xylose unit 3 makes a hydrogen bond to Ser41 and Gln254 in the complex with xylotriose, while only a hydrogen bond to Gln254 and water mediated contacts to this unit are observed in the xylohexose complex. Xylose unit 4 is engaged in contacts with Ala42, Gly45, Asp284, Lys283 and Phe350 (Fig. 5A).

Surprisingly, arabinohydroxylobiose and arabinohydroxylotriose bind with opposite directionalities. The binding pocket at position number 1 is occupied by the reducing end xylosyl of arabinohydroxylobiose but by the non-reducing end xylosyl of arabinohydroxylotriose (Fig. 5C and D). The arabinosyl moiety of arabinohydroxylobiose at position 2' makes van der Waals' contacts with Phe350 and is recognized by numerous polar contacts to Asn39, Ser144, Glu146, Thr318, Pro324 and Tyr346 (Fig. 6C). By contrast the arabinosyl moiety at position 1' in arabinohydroxylotriose is engaged in polar contacts with the backbone carbonyl oxygen of Asn72 and the amide nitrogen of Ala76 (Fig. 5D). The spacious binding pocket is filled with solvent molecules that mediate a network of hydrogen bonds, likely to make an important contribution to ligand binding (Fig. 5). Besides rearrangements in solvent, the main difference between the four complex structures is the conformational change in the loop region Ala40–Glu44 (lid loop) that blocks one end of the binding site in the xylotriose and arabinohydroxylotriose complexes, but is displaced outward upon binding the other two ligands with two mainchain hydrogen bonds between Ala42 and Gly45 and the xylosyl unit 4 in the xylohexose complex (Fig. 5).

Xylo-oligosaccharide uptake by *B. animalis* subsp. *lactis* BI-04

To assay for XOS uptake, *B. animalis* subsp. *lactis* BI-04 was grown in the presence of a XOS mixture and the xylose, xylobiose, xylotriose and xylohexose concentrations were monitored in the culture supernatant throughout the exponential growth phase. The depletion of xylotriose and xylohexose occurred in the mid-exponential phase, whereas xylobiose was still detected in the culture supernatant until the late log phase of growth suggesting that xylotriose and xylohexose were internalized more efficiently than xylobiose (Fig. 6).

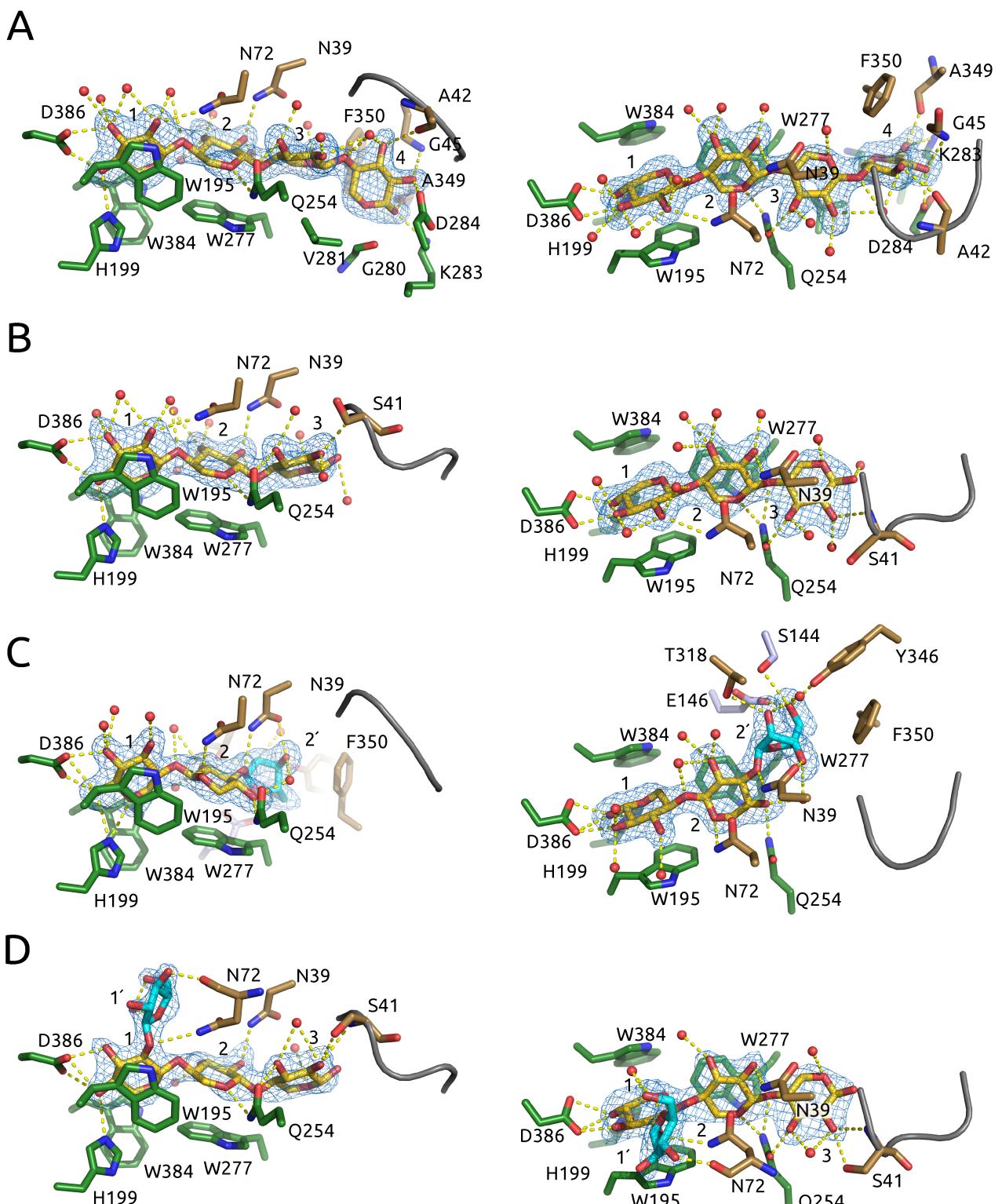


Fig. 5. Close-up of the *BAXBP* binding site in complex with (A) xylotetraose, (B) xylotriose, (C) arabinoxylobiose and (D) arabinoxylotriose shown in two orientations differing by a 90° rotation along the *x*-axis. Difference electron density maps calculated with coefficient $mF_{\text{obs}} - DF_{\text{calc}}$ and σ_A -weighted (contoured at 3σ) are shown as a light blue mesh. The lid loop that adopts different conformations depending on the ligand is depicted as a grey backbone trace of residues 40–44. Yellow dashes indicate polar interactions to protein atoms or water (red spheres). The main chain atoms are omitted for clarity unless they participate in polar interactions.

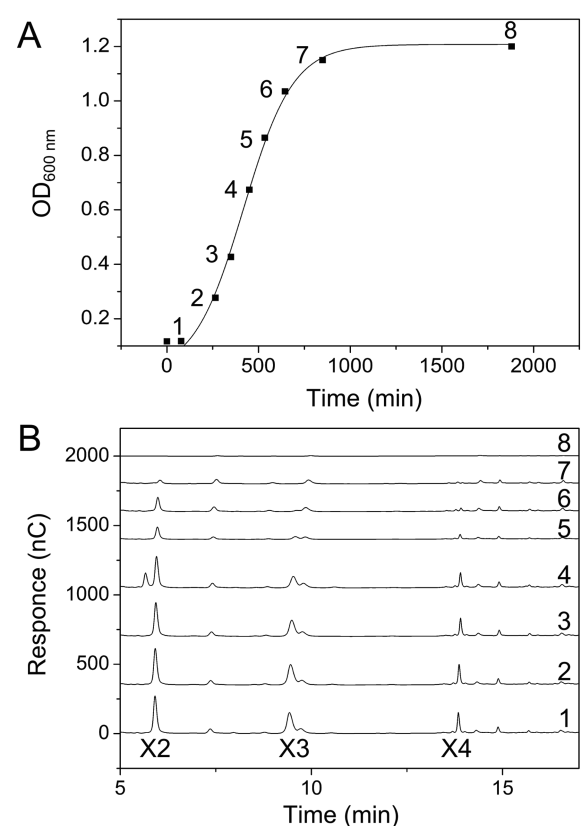


Fig. 6. Xylo-oligosaccharide uptake by uptake by *Bifidobacterium animalis* subsp. *lactis* BI-04.

A. Growth curve of *B. animalis* subsp. *lactis* BI-04 supplemented with 1% mixture xylo-oligosaccharide mixture. The numbers indicate sampling time points for OD₆₀₀ measurements and oligosaccharide analysis of culture supernatants. B. High-performance anion exchange chromatography with peramperometric detection (HPAEC-PAD) analysis of the fermentation supernatants with the same numbering as in (A). The peaks corresponding to, xylobiose (X2), xylotriose (X3) and xylotetraose (X4) standards are indicated.

Discussion

The preferential stimulation of distinct health-promoting groups from the gut microbiota by prebiotic oligosaccharides that are indigestible by the host is well established (Kolida and Gibson, 2011), and manipulation of the composition of the gut complex microbial community offers an attractive non-evasive strategy in treatment of pathogenic infections as well as metabolic and immune disorders. Molecular understanding of preferential microbial glycan utilization in the gut, however, remains elusive.

Transcriptional analyses have implicated a diversity of carbohydrate transport systems in uptake of oligosaccharides for intracellular degradation in probiotic bacteria (Andersen *et al.*, 2012; 2013) and the occurrence of certain ATP-binding cassette (ABC) carbohydrate transporters together with high acetate production in bifidobac-

terial strains have been correlated to probiotic traits such as protection from pathogenic infection in mice (Fukuda *et al.*, 2011). The present study reports the biochemical and structural features of the solute binding protein *BIA*XBP that mediates the capture of arabinoxylan oligomers within *Bifidobacterium*.

Capture and uptake of XOS and AXOS in bifidobacteria

The high affinity of *BIA*XBP to both undecorated and arabinosyl decorated xylo-oligosaccharides (Table 1, Fig. S1) is consistent with the growth of bifidobacteria on AXOS (van Laere *et al.*, 1999). The degradation of AXOS occurs intracellularly and proceeds by the removal of arabinosyl and acetyl substituents by specific GH43 arabinofuranosidases (van den Broek *et al.*, 2005) and acetyl esterases (Biely, 2012) respectively. This is followed by degradation of the xylo-oligosaccharide mainchain to xylose mainly by highly conserved GH43 β-xilosidases (> 78% amino acid sequence identity between the most distant sequences with *Bifidobacterium*) that are invariantly encoded in the bifidobacterial AXOS utilization loci (Fig. 7). Thus, the presence of transport systems is a prerequisite for the utilization of these glycans, and bifidobacteria are the only members of the gut microbiota that are currently known to produce an ABC transport system to mediate AXOS uptake. The amino acid sequences of the AXOS-specific SBP share high sequence identity within *Bifidobacterium* (ligand binding residues virtually identical, Fig. S5), and segregate mainly based on taxonomic distance (Fig. S6), indicating functional conservation.

Intracellular GH43 β-xilosidases and the ABC transporter constitute the core of the AXOS utilization system within *Bifidobacterium* as highlighted by the consistent colocalization of their genes together with one or more GH43 arabinofuranosidase and esterase genes within the AXOS operon (Fig. 7). Larger divergence is noted in arabinofuranosidase sequences as well as in the composition of hydrolases and esterases encoded in the AXOS operon between the different *Bifidobacterium* groups (Fig. 7). In summary, a highly conserved SBP confers the capture of XOS and AXOS in *Bifidobacterium* despite considerable variations in xylanolytic enzymes in different bifidobacterial groups.

Structural features, kinetics and thermodynamics of XOS recognition

In this study we have employed surface plasmon resonance to discern the kinetics of binding, whereas insight into the binding energetics was provided by isothermal titration calorimetry. The use of independent biophysical techniques to measure binding corroborated the binding constants rendering the data more reliable. The differ-

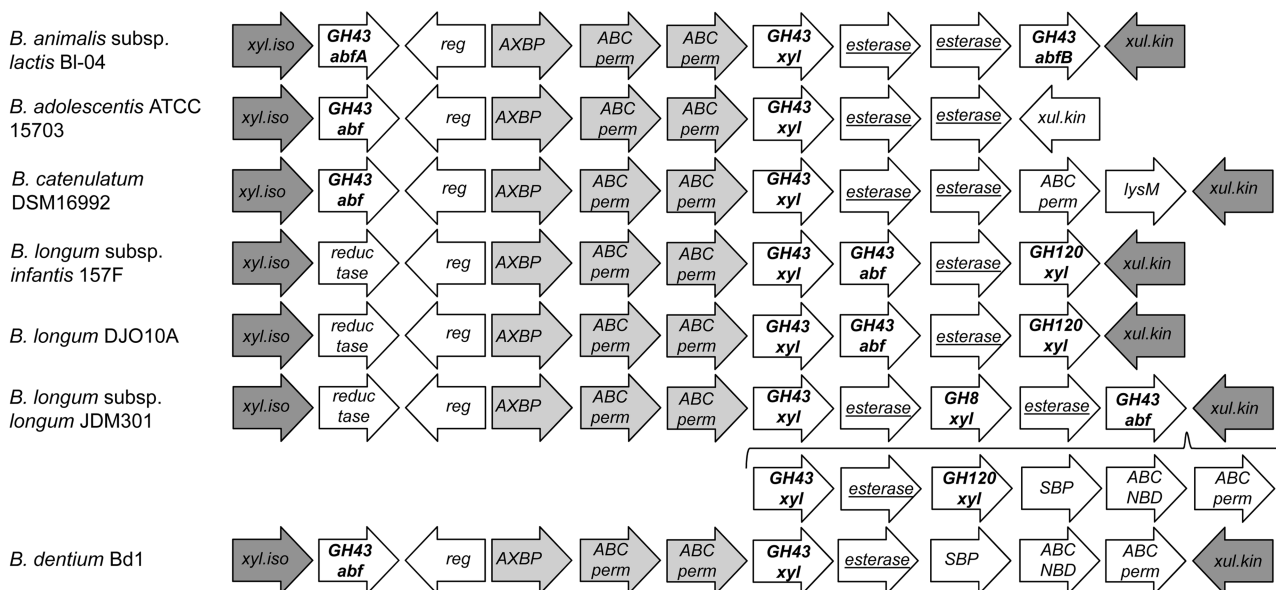


Fig. 7. Organization of the arabinoxyl-oligosaccharide utilization loci based on the annotated bifidobacterial genomes. The loci are aligned with respect to the AXOS-specific ABC transport system depicted in light grey and consisting of solute binding protein (AXBP) and two adjacent transmembrane domain genes (ABC perm). Genes are denoted depending on the function of their products as: glycoside hydrolases in bold, esterases (*esterase*) are underlined, the xylose metabolism genes xylose isomerase (*xyl.iso*) and xylulose kinase (*xul.kin*) are in dark grey. Conserved β -xylosidase genes of glycoside hydrolase family 43 (*GH43 xyl*) and LacI transcriptional regulators (*reg*) flank the AXOS-specific ABC transporter. Variations in the number and order of reductases, esterases, GH43 arabinofuranosidases (*GH43 abf*), GH8 and GH120 β -xylosidases (*GH8 xyl* and *GH120 xyl* respectively) are observed between the different *Bifidobacterium* groups. The *B. longum* group shows more complexity with respect to the number and types of xylanolytic genes and it has a long insertion including genes for a second ABC transport system of unknown specificity, comprising a solute binding protein (*SBP*), a nucleotide binding domain (*ABC NBD*) and a transmembrane domain (*ABC perm*). The presence of a second ABC transport system is also observed in *B. dentium* Bd1.

ences in affinity of *BIA*BP for various XOS ligands is determined largely by the association rate constant (k_{on}), while changes in the dissociation rate constant are modest except for xylobiose (Table 1, Fig. S1). The magnitude of the dissociation rate constant (k_{off}) reflects the short range interactions between the protein and the ligand, while k_{on} is influenced by diffusion, favourable electrostatics at the encounter complex distance (Sheinerman *et al.*, 2000), and molecular rearrangements associated with the binding event. The highest affinity measured towards xylotetraose is in excellent agreement with the structural data revealing a binding site large enough to accommodate this ligand. Thus, fewer interactions are possible with xylobiose compared to xylotriose or xylotetraose, rationalizing its 16-fold faster k_{off} compared to xylotetraose (Table 1, Fig. S1). Unsubstituted ligands longer than xylotetraose are likely to protrude out of the binding site without forming additional protein contacts, consistent with the essentially invariant k_{off} for xylotetraose through xylohexaose. The high affinity for non-reducing end arabinosyl substituents in arabinoxylobiase and arabinoxylotriose (Table 1) is consistent with the contribution of the additional interactions between the arabinosyl side-chains and the protein to the binding energy (Fig. 5C and D). Internal arabinosyl decorations as in arabinoxyltetraose are accommodated but are less

favoured as judged by the considerably slower association rate constant of arabinoxyltetraose as compared to xylo-tetraose. Similarly, the reduced affinity of xylobiose, xylopentoase and xylohexaose as compared to xylotetraose is mainly attributed to a reduction in k_{on} , which suggests that binding of these ligands is associated with a slower transition from the open to the closed conformation of the SBP (Björkman and Mowbray, 1998). Thus the ligand preference of *BIA*BP is fine-tuned mainly by the size of the association rate constant for optimal recognition of decorated and undecorated xylo-oligosaccharides with DP 3–4. Nonetheless, the lowest measured affinities for xylobiose and arabinoxyltetraose are in the micromolar range, suggesting that these ligands are likely to be transported and metabolized if they are available in sufficient concentrations. This is confirmed by the XOS uptake experiment, which showed that the preferred ligands xylotriose and xylotetraose are depleted before xylobiose (Fig. 7).

The thermodynamic signatures of xylotriose and xylo-tetraose capture by *BIA*BP were similar and revealed an enthalpically dominated binding, compensated by large entropic penalties in agreement with the structural data showing extensive direct and solvent mediated protein-ligand interactions (Fig. 5). The unfavourable entropy is likely to arise from the ordering of water molecules in the

binding pocket and the loss of conformational freedom of both the ligand and the protein sidechains and domains (Jelesarov and Bosshard, 1999) that possess rotational freedom along the hinge axis. The entropy of ordering the solvent molecules seems to be crucial in the entropic off-set of binding, as other glycan-specific solute binding proteins that lack ordered solvent in the binding pocket display significantly lower entropic compensation, e.g. the blood antigen binding protein from *Streptococcus pneumoniae* (Higgins *et al.*, 2009), which has an entropic penalty of binding energy mounting to ca 10% ΔH as compared to 76% for *BIA*BP. Conversely, the energetic fingerprint of *BIA*BP is similar to the lacto-N-biose binding SBP from *B. longum* (Suzuki *et al.*, 2008), which also employs ordered solvent molecules to mediate a hydrogen bonding network to the bound ligand.

*Structural plasticity of *BIA*BP*

Recently the xylo-oligosaccharide-specific binding protein from the thermophilic bacterium *C. polysaccharolyticus* has been structurally and biochemically characterized (Han *et al.*, 2012), and in addition biochemical data are available for the XOS-specific SBP from *Streptomyces thermophilic* (designated as BxIE) (Tsujibo *et al.*, 2004). Binding of arabinosyl decorated ligands was not shown for any of these SBPs, which exhibit a different ligand preference with the highest affinity skewed towards smaller ligands, e.g. xylobiose and xylotriose than observed for *BIA*BP. Also the kinetics of binding are different, as the magnitude of the dissociation rate constant governed the high affinity of BxIE towards xylobiose, while the association rate constant changes modulate the selection of *BIA*BP towards xylotetraose. The most striking difference, however, between *BIA*BP and the counterpart from *C. polysaccharolyticus* is the considerably higher structural plasticity of the bifidobacterial protein manifested in the ability to recognize xylo-oligosaccharides with diverse size and arabinosyl substitutions (Table 1, Fig. 5, Fig. S7). This striking plasticity is the result of different modes of binding of decorated and undecorated ligands, which is facilitated by the similar structure of xylo-oligosaccharides bound in opposite directionalities and recognition of arabinosyl substituents at two different positions of ligands bound with different directionalities (Fig. 5, Fig. S4). Additionally, *BIA*BP possesses a more spacious pocket featuring internal cavities, which are filled with solvent molecules. These solvent molecules are rearranged based on bound ligand to mediate a hydrogen bonding network between the ligand and the protein. The spaciousness of the pocket in *BIA*BP is effectuated by the lack of several bulky residues responsible for the narrow active site in the homologue from *C. polysaccharolyticus* (Fig. S8). A lid loop which is conformationally flexible to

accommodate different ligands further contributes to the plasticity of the ligand binding site.

*Biological implications of the ligand preference of *BIA*BP: xylan catabolism in the gut*

Plant cell wall polysaccharides, including arabinoxylan fibres that are abundant in human diet, provide the gut microbiota with an important metabolic resource. Members of the dominant *Bacteroides* genus and *Roseburia* species that possess modular GH10 endo-xylanases featuring catalytic modules appended to one or more xylan binding modules are reported as the prevalent xylanolytic taxa in the gut (Mirande *et al.*, 2010). Xylan is captured and hydrolysed into large fragments that are subsequently transported via the SusC transport protein in *Bacteroides* (Dodd *et al.*, 2011). The capture of xylan fragments in *Bacteroides* is effectuated by xylan binding domains, which typically display lower affinities on ligands smaller than xylohexose (McCartney *et al.*, 2006). Only xylan oligomers larger than a xylopentaose were reported to induce the xylanolytic system in *Bacteroides* (Mirande *et al.*, 2010), which asserts the preference of *Bacteroides* for larger xylan fragments and suggests uptake of smaller ligands is less efficient. This specialization provides a possible rationale for the preference of bifidobacteria to exploit complementary substrate sizes, which avoids competition with dominant specialized xylan degrading taxa. Xylan degradation occurs mainly in the proximal colon (Pochart *et al.*, 1993). Thus a gradient of increasing concentration of smaller xylo-oligosaccharides is likely to be formed downstream in the colon, providing a niche for bifidobacteria and other taxa with efficient XOS uptake and utilization systems. Only a few Firmicutes, e.g. *L. brevis* are reported to grow on XOS (Moura *et al.*, 2007). The XOS utilization system in these organisms is much simpler as judged from the genetic loci encoding a transcriptional regulator, a GH43 putative β -xylosidase and a major facilitator superfamily permease (e.g. *L. brevis* ATCC 367 and *Weissella korensis* KACC 15510). The fine-tuning of XOS capture towards larger ligands than xylobiose, and towards arabinosyl decorated ligands may provide a competitive advantage for bifidobacteria over Firmicutes that are unable to utilize such ligands. This is consistent with the *in vitro* uptake experiments performed in this study, showing that the disaccharide xylobiose was taken up with lower efficiency than the tri- and tetrasaccharide counterparts.

Niche adaptation is evident upon comparison of *BIA*BP with the counterparts from *S. thermophilic* isolated from decayed wood and *C. polysaccharolyticus* isolated from hot spring sediment. Both *S. thermophilic* and *C. polysaccharolyticus* are capable of producing extracellular endoxylanases that generate mainly short XOS of DP 2–3 (McCarthy and Williams, 1992; Han *et al.*,

2012) and their uptake proteins are optimized for this size of substrate. By contrast, *B. animalis* subsp. *lactis* and the majority of AXOS utilizing bifidobacterial strains rely on efficient capture to cross-feed from primary arabinoxylan degraders, e.g. *Roseburia* and *Bacteroides* in the densely populated colon.

The high specialization and complementary substrate preference evolved to avoid competition among dominant commensals are likely to be important niche adaptation mechanisms that establish metabolic syntrophy (cross-feeding) among the gut microbiota.

This study provides novel insight into the molecular features responsible for the impressive versatility of the first arabinxylo-oligosaccharide binding protein to be described and advances our understanding of the complex metabolic interplay and competition that play a key role in defining our gut microbiota.

Experimental procedures

Chemicals

All chemicals were of analytical grade. The following carbohydrate ligands were used: XOS Longlive 95P (84% xylo-oligosaccharides composed of 43% xylobiose, 30% xylotriose, 10% xylotetraose, 17% DP \geq xylpentose, 13.5% other monosaccharides) described in Mäkeläinen *et al.* (2010). Xylo-oligosaccharides xylobiose–xylotetraose > 95%, xylopentaose and xylohexose ~ 95% were from Megazyme (Wicklow, Ireland). Arabinxylo-oligosaccharides, with DP 3–5 (~ 95% pure) were a kind gift of Dr Barry McCleary (Megazyme): arabinxylobiose: [α -L-Araf-(1,3)]- β -D-Xylp-(1,4)-D-Xylp; arabinxylotriose: mixture of [α -L-Araf-(1,2)]- β -D-Xylp-(1,4)-D-Xylp-(1,4)-D-Xylp (90%) + β -D-Xylp-(1,4)-[α -L-Araf-(1,3)]- β -D-Xylp-(1,4)-D-Xylp (10%); arabinxylotetraose: β -D-Xylp-(1,4)-[α -L-Araf-(1,3)]- β -D-Xylp-(1,4)- β -D-Xylp-(1,4)-D-Xylp (80%) + β -D-Xylp-(1,4)-[α -L-Araf-(1,2)]- β -D-Xylp-(1,4)- β -D-Xylp-(1,4)-D-Xylp (20%) (see Fig. 1 for the chemical structures of these ligands). Xylose, sucrose, cellobiose, melibiose, isomaltose, raffinose, fructo-oligosaccharides from chicory (DP 2–60 average of 10), were > 98% pure (Sigma-Aldrich, St. Louis, MO, USA). Purified (95% purity) β -galactooligosaccharide mixture (GOS) with DP 2–6 was kindly provided by Dr S. Lahtinen (DuPont Nutrition and Health, Kantvik, Finland).

Cloning, expression and purification of the arabinxylo-oligosaccharide binding protein from *B. animalis* subsp. *lactis* BI-04 (BIAxBP)

Chromosomal DNA of *B. animalis* subsp. *lactis* BI-04 (Barrangou *et al.*, 2009) (kindly provided by DuPont Nutrition & Health, Madison, WI, USA) was isolated according to Sambrook and Russell (2006). The gene fragment encoding the xylo-oligosaccharide SBP of the ATP-binding cassette (ABC) transporter in the XOS utilization operon (locus tag number, *balac_0514*, GenBank Accession No. NC_01281; 609361.610638; GI:241190066) without the signal peptide predicted by SignalP v.3.0 (Bendtsen *et al.*, 2004) (basepairs

1–54) was cloned using the sense primer: 5'-CTAGCTA GCATGAGCGCATGTGGCGGG-3' and antisense primer: 5'-CCGGAGCTCTCAGCCCTTCTGGCGGG-3' and the TaKaRa PrimeStar high GC PCR kit (Takara Bio, Otsu, Shiga, Japan) between the Nhel and Xhol restriction sites (bold) in pET28a(+) (Novagen, Darmstadt, Germany) to yield the expression vector pET28aBalac_0514, which was transformed into *E. coli* DH5 α and selected on LB plates supplemented with 50 μ g ml $^{-1}$ kanamycin. Following restriction analysis and full sequencing, pET28aBalac_0514 was transformed into *E. coli* BL21(DE3) and B834DE3 (Novagen) for expression of unlabelled and selenomethionine labelled protein respectively. The recombinant AXOS binding protein designated as BIAxBP, was produced as an N-terminal fusion of a thrombin cleavable hexa-histidine tag with the BIAxBP mature polypeptide lacking the native transit peptide (amino acid residues 1–18), but having a six amino acid insertion (GSHMAS) between the N-terminus of the protein and the tag cleavage site.

Escherichia coli BL21(DE3) cells harbouring pET28Balac_0514 were used to produce BIAxBP in a 5 l Biostat B bioreactor (B. Braun Biotech International, Melsungen, Germany) as previously described (Fredslund *et al.*, 2011) except that OD $_{600}$ for induction was 7. Selenomethionine labelled BIAxBP was produced in B834DE3 according to Studts and Fox (1999). Cell harvest, disruption and his-tag affinity purification was carried out according to Fredslund *et al.* (2011). Fractions containing BIAxBP, identified by SDS-PAGE, were concentrated, loaded onto a gel filtration HiLoad Superdex 200 16/60 column (GE Healthcare) and eluted with 10 mM MES 150 mM NaCl, pH 6.5 at 1 ml min $^{-1}$. BIAxBP-containing fractions were pooled, concentrated, dialysed against 10 mM MES, pH 6.5, applied onto a 6 ml anion exchange Resource Q column (GE Healthcare) and eluted by a three step NaCl gradient yielding ~ 2.5 mg homogenous BIAxBP per g cell pellet. Chromatographic steps were performed using an AKTA-AVANT chromatograph (GE Healthcare) at 4°C. The His tag was removed using human thrombin (Calbiochem, Merck, Darmstadt, Germany) as recommended by the manufacturer. The protein concentration was determined by measuring A_{280} using a molar extinction coefficient $\epsilon_{280} = 78921 \text{ M}^{-1} \text{ cm}^{-1}$ determined experimentally by aid of amino acid analysis (Barkholt and Jensen, 1989), comparable to the calculated value of $\epsilon_{280} = 66140 \text{ M}^{-1} \text{ cm}^{-1}$.

Surface plasmon resonance (SPR)

Affinity of BIAxBP for the different xylo-oligosaccharides was determined using a Biacore T100 (GE Healthcare). BIAxBP, diluted into 10 mM sodium acetate pH 4.1 to 2.3 μ M, was immobilized on a CM5 sensor chip using a random amine coupling kit (GE Healthcare) to a density of 2900 response units (RU). Sensograms were recorded at 25°C in 20 mM phosphate/citrate buffer; 150 mM NaCl; pH 6.5, 0.005% (v/v) P20 surfactant (GE Healthcare) at a flow of 30 μ l min $^{-1}$ with association and dissociation times of 90 s and 240 s respectively. Experiments were performed in triplicates in the range 3 nM–10 μ M for xylotriose–xylpentose, 5 nM–1 μ M AXOS ligands and 0.5 μ M–1 mM for xylobiose and xylotetraose, all dissolved in the same buffer as above. To investigate the ligand specificity of BIAxBP, binding was tested towards

5 mM xylose, cellobiose, raffinose, sucrose, melibiose, iso-maltose, FOS and GOS in the same buffer. The affinity of *B*/AXBP for xylotetraose was investigated at eight different pH values in the range pH 3–9, while dependence of binding on temperature was examined in the range 15–30°C. Data analysis was carried out using the Biacore T100 evaluation software, and equilibrium dissociation constants (K_d) were calculated by fitting a one site binding model to either the steady-state response data or the full sensograms to measure the binding kinetics. Stoichiometry (n) of *B*/AXBP binding was determined by the equation:

$$n = \frac{R_{\max} \cdot MW_1}{MW_a \cdot R_i}$$

where R_{\max} (analyte maximum binding capacity) is obtained from the fits to the individual data sets and R_i is the attained immobilization level, MW_1 and MW_a are the molecular masses of the immobilized protein and carbohydrate analyte respectively (Morton and Myszka, 1998). This stoichiometry is underestimated due to the inactivation of a certain proportion of the protein concomitant with the immobilization procedure.

Isothermal titration calorimetry (ITC)

Binding of xylotriose and xylotetraose to *B*/AXBP in 10 mM sodium phosphate pH 6.5 was measured at 25°C using an ITC₂₀₀ microcalorimeter (MicroCal). *B*/AXBP (14 or 25 μM) in the sample cell (200 μl) was titrated by a first injection of 0.5 μl followed by 18 × 2 μl injections of carbohydrate ligand (140 or 250 μM) with 120 s between injections. Data were analysed using the MicroCal software (Wiseman *et al.*, 1989).

Fluorescence titration spectroscopy

Intrinsic tryptophan emission was measured on a Spex Fluorlog 322 fluorescence spectrometer (HORIBA Jobin Yvon, Irvine, CA, USA) in a 1 ml stirred quartz cuvette at 25°C. Purified *B*/AXBP diluted to 4 μM in 10 mM sodium phosphate pH 6.5 and pre-equilibrated for 5 min was titrated with 0.5 μl of 0.5 mM of xylotriose or xylotetraose. Instrument settings and data analysis were as previously reported (Erkens and Slotboom, 2010). The ligand-specific contribution to fluorescence quenching was corrected for in all measurements.

Crystallization and structure determination

Initial crystallization conditions (0.1 M Tris pH 7, 40% PEG-300 and 5% PEG-1000 at 278 K) was found using the Cryo crystallization screen (Emerald BioSystems, MA, USA), using a Mosquito® liquid handling robot (TTP Labtech, UK). *B*/AXBP and selenomethionine labelled *B*/AXBP (15 mg·ml⁻¹ in 10 mM MES pH 6.5 and 150 mM NaCl) was co-crystallized with xylo-oligosaccharides (1 mM) using vapour diffusion in either sitting or hanging drops and grew for 30 h at 5°C at a 1:1 ratio of *B*/AXBP and reservoir solution. Xylotriose and xylotetraose complexes were grown with a reservoir solution of 0.1 M Tris pH 7.5, 47% PEG 300 and 5% PEG 1000, while complexes with arabinosylobiose and arabinosylotriose were obtained with a reservoir solution of 0.1 M Tris pH 7.0, 40% PEG 300 and 5% PEG 1500. Due to the high concentrations of PEG in

the reservoir solution no further cryo-protectant was needed and the crystals were flash frozen directly in liquid nitrogen. Diffraction data were collected to a maximum resolution of 3.1 Å for selenomethionine labelled *B*/AXBP:xylotetraose complex, 2.0 Å for *B*/AXBP:arabinosylobiose complex, 2.4 Å for *B*/AXBP:arabinosylotriose complex, 2.2 Å for *B*/AXBP:xylotetraose complex and 2.4 Å for *B*/AXBP:xylotriose complex at the SLS beamlines PXI and PXIII, Villigen, Switzerland and MAX-LAB, Lund, Sweden (see Table 3). All data sets were processed with XDS (Kabsch, 2010). The structure of selenomethionine *B*/AXBP was solved in the orthorhombic space group *P*2₁ 2₁ 2 using the single-anomalous diffraction (SAD) method with the experimental phase information obtained from data collected at the Selenium K-edge. The program Phenix.AutoSol (McCoy *et al.*, 2007; Adams *et al.*, 2010) identified 15 out of 17 selenomethyl residues present in the *B*/AXBP. An initial partial model was obtained with Phenix.AutoBuild (Terwilliger, 2004) and further corrections and model building using the program Coot (Emsley and Cowtan, 2004) resulted in a 75% complete model, which was used in molecular replacement to solve the structure of *B*/AXBP:xylotetraose. The model was completed using automatic and manual model building and refined using phenix.refine (Afonine *et al.*, 2012) randomly setting aside 5% of the reflections. Molecular replacement with the protein part of *B*/AXBP:xylotetraose was used to solve *B*/AXBP:xylotriose, *B*/AXBP:arabinosylobiose and *B*/AXBP:arabinosylotriose complexes. Ligand molecules were included after the protein parts were build and water molecules were added with Coot or manually. The overall quality of all models was checked using MolProbity (Chen *et al.*, 2010). The final models of *B*/AXBP in complex with arabinosylobiose, arabinosylotriose, xylotriose and xylotetraose were refined to $R_{\text{cryst}}/R_{\text{free}}$ values of 0.15/0.20, 0.21/0.25, 0.20/0.24 and 0.19/0.24 respectively. The models are deposited in the Protein Data Bank (PDB) with accession codes 4c1u (arabinosylobiose complex), 4c1t (arabinosylotriose complex), 3zkl (xylotriose complex) and 3zkk (xylotetraose complex). The four complexes are very similar in conformation and superposition of the individual models results in pairwise overall RMSDs between 0.3 and 0.6 Å between aligned C_α atoms. The PyMOL Molecular Graphics System, Version 1.5.0.3 Schrödinger, LLC was used to explore the models and for rendering. The linkage torsion angles of the XOS ligands were examined using the carp tool available at <http://www.glycosciences.de/tools/carp/>.

In vivo XOS uptake

Bifidobacterium animalis subsp. *lactis* BI-04 was grown at 37°C in LAB SEM media (Barrangou *et al.*, 2003) supplemented with 1% (w/v) XOS (Longlive 95P) under anaerobic conditions. Growth was monitored by measuring A_{600} ; samples were collected during the exponential growth phase and immediately chilled to 0°C. The supernatants after centrifugation were collected and sterile filtered before HPAEC-PAD analysis.

Xylo-oligosaccharides present in culture supernatants were analysed by high-performance anion exchange chromatography with pulsed amperometric detection (HPAEC-PAD) (Dionex, California, USA) using a CarboPac PA200 column and a mobile phase (0.35 ml min⁻¹) of constant 100 mM

NaOH and a gradient of sodium acetate 0–20 min of 0–160 mM and 20–25 min of 160–400 mM. Standards of xylose (Merck, Germany), xylobiase, xylotriose and xylo-tetraose (Megazyme, Wicklow, Ireland) were used to identify the peaks in the chromatograms using 10 µl injections. Samples were diluted in 10× in MQ water and subsequently 10× in 100 mM NaOH before analysis and compared with the standards.

Acknowledgements

This research was funded by a FøSu grant from the Danish Strategic Research Council to the project 'Gene discovery and molecular interactions in pre/probiotics systems. Focus on carbohydrate prebiotics'; an instrument grant from the Danish Council for Independent Research | Natural Sciences for Biacore T100; a PhD stipend from the Technical University of Denmark (to M.E.); A.V.-Z. and D.J.S. were supported by the European Union (European Research Council starting grant to D.J.S. and EDICT programme) and the Netherlands Organisation for Scientific Research (NWO). Mette Pries and Birgit Andersen are thanked for technical assistance and advice with the production of the selenomethionine labelled protein and help with HPAEC-PAD analysis. Anne Blicher is thanked for amino acid analysis. We are grateful to Dr Sampo Lahtinen (DuPont Nutrition and Health, Kantvik, Finland) and to Dr Barry McCleary (Megazyme) for kind gifts of GOS and AXOS samples respectively.

References

- Adams, P.D., Afonine, P.V., Bunkoczi, G., Chen, V.B., Davis, I.W., Echols, N., et al. (2010) PHENIX: a comprehensive Python-based system for macromolecular structure solution. *Acta Crystallogr D Biol Crystallog* **66**: 213–221.
- Afonine, P.V., Grosse-Kunstleve, R.W., Echols, N., Headd, J.J., Moriarty, N.W., Mustyakimov, M., et al. (2012) Towards automated crystallographic structure refinement with phenix.refine. *Acta Crystallogr D Biol Crystallog* **68**: 352–367.
- Andersen, J.M., Barrangou, R., Abou Hachem, M., Lahtinen, S.J., Goh, Y.J., Svensson, B., and Klaenhammer, T.R. (2012) Transcriptional analysis of prebiotic uptake and catabolism by *Lactobacillus acidophilus* NCFM. *PLoS ONE* **7**: e44409.
- Andersen, J.M., Barrangou, R., Abou Hachem, M., Lahtinen, S., Goh, Y.J., Svensson, B., and Klaenhammer, T.R. (2013) Transcriptional analysis of oligosaccharide utilization by *Bifidobacterium lactis* BI-04. *BMC Genomics* **14**: 312.
- Arumugam, M., Raes, J., Pelletier, E., Le Paslier, D., Yamada, T., Mende, D.R., et al. (2011) Enterotypes of the human gut microbiome. *Nature* **473**: 174–180.
- Barkholt, V., and Jensen, A.L. (1989) Amino-acid analysis – determination of cysteine plus half-cysteine in proteins after hydrochloric-acid hydrolysis with disulphide compound as additive. *Anal Biochem* **177**: 318–322.
- Barrangou, R., Altermann, E., Hutchins, R., Cano, R., and Klaenhammer, T.R. (2003) Functional and comparative genomic analyses of an operon involved in fructooligosaccharide utilization by *Lactobacillus acidophilus*. *Proc Natl Acad Sci USA* **100**: 8957–8962.
- Barrangou, R., Briczinski, E.P., Traeger, L.L., Loquasto, J.R., Richards, M., Horvath, P., et al. (2009) Comparison of the complete genome sequences of *Bifidobacterium animalis* subsp. *lactis* DSM 10140 and BI-04. *J Bacteriol* **191**: 4144–4151.
- Benttsen, J.D., Nielsen, H., von Heijne, G., and Brunak, S. (2004) Improved prediction of signal peptides: SignalP 3.0. *J Mol Biol* **340**: 783–795.
- Berntsson, R.P.A., Smits, S.H.J., Schmitt, L., Slotboom, D.J., and Poolman, B. (2010) A structural classification of substrate-binding proteins. *FEBS Lett* **584**: 2606–2617.
- Biely, P. (2012) Microbial carbohydrate esterases deacetylating plant polysaccharides. *Biotechnol Adv* **30**: 1575–1588.
- Björkman, A.J., and Mowbray, S.L. (1998) Multiple open forms of ribose-binding protein trace the path of its conformational change. *J Mol Biol* **279**: 651–664.
- van den Broek, L.A.M., Lloyd, R.M., Beldman, G., Verdoes, J.C., McCleary, B.V., and Voragen, A.G.J. (2005) Cloning and characterization of arabinoxylan arabinofuranohydro-lase-D3 (AXhd3) from *Bifidobacterium adolescentis* DSM20083. *Appl Microbiol Biotechnol* **67**: 641–647.
- Chen, V.B., Arendall, W.B., Headd, J.J., Keedy, D.A., Immormino, R.M., Kapral, G.J., et al. (2010) MolProbity: all-atom structure validation for macromolecular crystallography. *Acta Crystallogr D Biol Crystallog* **66**: 12–21.
- Crittenden, R., Karppinen, S., Ojanen, S., Tenkanen, M., Fagerstrom, R., Matto, J., et al. (2002) *In vitro* fermentation of cereal dietary fibre carbohydrates by probiotic and intestinal bacteria. *J Sci Food Agric* **82**: 781–789.
- Davidson, A.L., Dassa, E., Orelle, C., and Chen, J. (2008) Structure, function, and evolution of bacterial ATP-binding cassette systems. *Microbiol Mol Biol Rev* **72**: 317–364.
- Dodd, D., Mackie, R.I., and Cann, I.K. (2011) Xylan degradation, a metabolic property shared by rumen and human colonic Bacteroidetes. *Mol Microbiol* **79**: 292–304.
- Eckburg, P.B., Bik, E.M., Bernstein, C.N., Purdom, E., Dethlefsen, L., and Sargent, M. (2005) Diversity of the human intestinal microbial flora. *Science* **308**: 1635–1638.
- Emsley, P., and Cowtan, K. (2004) Coot: model-building tools for molecular graphics. *Acta Crystallogr D Biol Crystallog* **60**: 2126–2132.
- Erkens, G.B., and Slotboom, D.J. (2010) Biochemical characterization of ThiT from *Lactococcus lactis*: a thiamin transporter with picomolar substrate binding affinity. *Biochemistry* **49**: 3203–3212.
- Flint, H.J., Duncan, S.H., Scott, K.P., and Louis, P. (2007) Interactions and competition within the microbial community of the human colon: links between diet and health. *Environ Microbiol* **9**: 1101–1111.
- Fredslund, F., Abou Hachem, M., Larsen, R.J., Sorensen, P.G., Coutinho, P.M., Leggio Lo, L., and Svensson, B. (2011) Crystal structure of α -galactosidase from *Lactobacillus acidophilus* NCFM: insight into tetramer formation and substrate binding. *J Mol Biol* **412**: 466–480.
- Fukuda, S., Toh, H., Hase, K., Oshima, K., Nakanishi, Y., and Yoshimura, K. (2011) Bifidobacteria can protect from enteropathogenic infection through production of acetate. *Nature* **469**: 543–549.
- Han, Y., Agarwal, V., Dodd, D., Kim, J., Bae, B., Mackie, R.I., et al. (2012) Biochemical and structural insights into xylan

- utilization by the thermophilic bacterium *Caldanaerobius polysaccharolyticus*. *J Biol Chem* **287**: 34946–34960.
- Hansen, C.H.F., Frokiaer, H., Christensen, A.G., Bergstrom, A., Licht, T.R., Hansen, A.K., and Metzdorff, S.B. (2013) Dietary xylooligosaccharide downregulates IFN- γ and the low-grade inflammatory cytokine IL-1 β systemically in mice. *J Nutr* **143**: 533–540.
- Higgins, M.A., Whitworth, G.E., El Warry, N., Randriantsoa, M., Samain, E., Burke, R.D., et al. (2009) Differential recognition and hydrolysis of host carbohydrate antigens by *Streptococcus pneumoniae* family 98 glycoside hydrolases. *J Biol Chem* **284**: 26161–26173.
- Holm, L., and Rosenström, P. (2010) Dali server: conservation mapping in 3D. *Nucleic Acids Res* **38**: 545–549.
- Jelesarov, I., and Bosshard, H.R. (1999) Isothermal titration calorimetry and differential scanning calorimetry as complementary tools to investigate the energetics of biomolecular recognition. *J Mol Recognit* **12**: 3–18.
- Kabsch, W. (2010) XDS. *Acta Crystallogr D Biol Crystallogr* **66**: 125–132.
- Kleerebezem, M., and Vaughan, E.E. (2009) Probiotic and gut lactobacilli and bifidobacteria: molecular approaches to study diversity and activity. *Annu Rev Microbiol* **63**: 269–290.
- Kolida, S., and Gibson, G.R. (2011) Synbiotics in health and disease. *Annu Rev Food Sci Technol* **2**: 373–393.
- Koropatkin, N.M., Cameron, E.A., and Martens, E.C. (2012) How glycan metabolism shapes the human gut microbiota. *Nat Rev Microbiol* **10**: 323–335.
- McCarthy, A.J., and Williams, S.T. (1992) Actinomycetes as agents of biodegradation in the environment – a review. *Gene* **115**: 189–192.
- McCartney, L., Blake, A.W., Flint, J., Bolam, D.N., Boraston, A.B., Gilbert, H.J., and Knox, J.P. (2006) Differential recognition of plant cell walls by microbial xylan-specific carbohydrate-binding modules. *Proc Natl Acad Sci USA* **103**: 4765–4770.
- McCoy, A.J., Grosse-Kunstleve, R.W., Adams, P.D., Winn, M.D., Storoni, L.C., and Read, R.J. (2007) Phaser crystallographic software. *J Appl Crystallogr* **40**: 658–674.
- Mäkeläinen, H., Forssten, S., Saarinen, M., Stowell, J., Rautonen, N., and Ouwehand, A. (2010) Xylo-oligosaccharides enhance the growth of bifidobacteria and *Bifidobacterium lactis* in a simulated colon model. *Benef Microbes* **1**: 81–91.
- Mirande, C., Kadlecikova, E., Matulova, M., Capek, P., Bernalier-Donadille, A., Forano, E., and Bera-Maillet, C. (2010) Dietary fibre degradation and fermentation by two xylanolytic bacteria *Bacteroides xylofasciens* XB1A and *Roseburia intestinalis* XB6B4 from the human intestine. *J Appl Microbiol* **109**: 451–460.
- Morton, T.A., and Myszka, D.G. (1998) Kinetic analysis of macromolecular interactions using surface plasmon resonance biosensors. *Methods Enzymol* **295**: 268–294.
- Moura, P., Barata, R., Carvalheiro, F., Giro, F., Loureiro-Dias, M.C., and Esteves, M.P. (2007) *In vitro* fermentation of xylo-oligosaccharides from corn cobs autohydrolysis by *Bifidobacterium* and *Lactobacillus* strains. *LWT-Food Sci Technol* **40**: 963–972.
- Nieduszynski, I., and Marchessault, R.H. (1971) Structure of β -D-(1→4')xylan hydrate. *Nature* **232**: 46–47.
- Nyman, M., Siljestrom, M., Pedersen, B., Knudsen, K.E.B., Asp, N.G., Johansson, C.G., and Eggum, B.O. (1984) Dietary fiber content and composition in 6 cereals at different extraction rates. *Cereal Chem* **61**: 14–19.
- Palframan, R., Gibson, G.R., and Rastall, R.A. (2003) Development of a quantitative tool for the comparison of the prebiotic effect of dietary oligosaccharides. *Lett Appl Microbiol* **37**: 281–284.
- Picard, C., Fioramonti, J., Francois, A., Robinson, T., Neant, F., and Matuchansky, C. (2005) Review article: Bifidobacteria as probiotic agents – physiological effects and clinical benefits. *Aliment Pharmacol Ther* **22**: 495–512.
- Pochart, P., Lemann, F., Flourié, B., Pellier, P., Goderel, I., and Rambaud, J.C. (1993) Pyrographic sampling to enumerate methanogens and anaerobes in the right colon of healthy humans. *Gastroenterology* **105**: 1281–1285.
- Sambrook, J., and Russell, D.W. (2006) Purification of nucleic acids by extraction with phenol:chloroform. *Cold Spring Harb Protoc* **2006**: pdb.prot4455.
- Sheinerman, F.B., Norel, R., and Honig, B. (2000) Electrostatic aspects of protein–protein interactions. *Curr Opin Struct Biol* **10**: 153–159.
- Studts, J.M., and Fox, B.G. (1999) Application of fed-batch fermentation to the preparation of isotopically labeled or selenomethionyl-labeled proteins. *Protein Expr Purif* **16**: 109–119.
- Suzuki, R., Wada, J., Katayama, T., Fushinobu, S., Wakagi, T., Shoun, H., et al. (2008) Structural and thermodynamic analyses of solute-binding protein from *Bifidobacterium longum* specific for core 1 disaccharide and lacto-N-biose I. *J Biol Chem* **283**: 13165–13173.
- Terwilliger, T. (2004) SOLVE and RESOLVE: automated structure solution, density modification, and model building. *J Synchrotron Radiat* **11**: 49–52.
- Tsuji, H., Kosaka, M., Ikenishi, S., Sato, T., Miyamoto, K., and Inamori, Y. (2004) Molecular characterization of a high-affinity xylobiose transporter of *Streptomyces thermophilus* OPC-520 and its transcriptional regulation. *J Bacteriol* **186**: 1029–1037.
- Van Laere, K.M.J., Voragen, C.H.L., Kroef, T., van den Broek, L.A.M., Beldman, G., and Voragen, A.G.J. (1999) Purification and mode of action of two different arabinoxylan arabinofuranohydrolases from *Bifidobacterium adolescentis* DSM 20083. *Appl Microbiol Biotechnol* **51**: 606–613.
- Wallace, T.C., Guarner, F., Madsen, K., Cabana, M.D., Gibson, G., Hentges, E., and Sanders, M.E. (2011) Human gut microbiota and its relationship to health and disease. *Nutr Rev* **69**: 392–403.
- Wiseman, T., Williston, S., Brandts, J.F., and Lin, L.N. (1989) Rapid measurement of binding constants and heats of binding using a new titration calorimeter. *Anal Biochem* **179**: 131–137.
- Xu, J., Mahowald, M.A., Ley, R.E., Lozupone, C.A., Hamady, M., Martens, E.C., et al. (2007) Evolution of symbiotic bacteria in the distal human intestine. *PLoS Biol* **5**: 1574–1586.

Supporting information

Additional supporting information may be found in the online version of this article at the publisher's web-site.